REPORT DOCUMENTATION PAGE

Form Approved
OMB No 0704-0188

1. AGENCY USE ONLY (LEAVE BLANK)	2. REPORT DATE	3. REPORT TYPE AND DATES COVERED
	May 1996	Technical Paper

4. TITLE AND SUBTITLE

Structural/Ballistic Instability Ageout Mechanism in the Sparrow Mark 52 SRM

5. FUNDING NUMBERS

C: In-House
PE: 62601F
PR: 3059
TA: RD63

6. AUTHOR(S)

D.I. Thrasher and P.R. Empleo

7. PERFORMING ORGANIZATION NAME(S) AND ADDRESS(ES)

Phillips Laboratory
OL-AC PL/RKEM
4 Draco Drive
Edwards AFB CA 93524-7190

8. PERFORMING ORGANIZATION REPORT NUMBER

PL-TP-96-3047

9. SPONSORING/MONITORING AGENCY NAME(S) AND ADDRESS(ES)

10. SPONSORING/MONITORING AGENCY REPORT NUMBER

11. SUPPLEMENTARY NOTES Pat Empleo works for Sparta, Inc., 244 E. Ave. K-4, Lancaster CA 93535

COSATI CODE(S): 2108; 210902

12a. DISTRIBUTION/AVAILABILITY STATEMENT

Approved for Public Release; Distribution is Unlimited

Presented at the NATO AGARD symposium on Service Life of Solid Propellant Systems, 6-10 May 1996, Athens, Greece

12b. DISTRIBUTION CODE

A

13. ABSTRACT (MAXIMUM 200 WORDS)

A three dimensional finite element analysis and a one dimensional incompressible flow model were used to investigate the interaction between the internal ballistics and the structural grain deformations for the Sparrow Mark 52 rocket motor. The results confirm earlier investigators' conclusions (based on two dimensional structural analysis) that a mechanism exists for pressure spiking driven by choking of the gas flow within the bore cavity due to grain structural deformations. Significant differences were found between the 2D and 3D results, however; the 3D analysis requires a higher propellant modulus to prevent choking under the same analysis conditions.

14. SUBJECT TERMS

solid propellant; structural/ballistic instability; Mark 52; solid rocket motor; Sparrow Mark 52; rocket motor; finitie element analysis

15. NUMBER OF PAGES

7

16. PRICE CODE

17. SECURITY CLASSIFICATION OF REPORT	18. SECURITY CLASSIFICATION OF THIS PAGE	19. SECURITY CLASSIFICATION OF ABSTRACT	20. LIMITATION OF ABSTRACT
Unclassified	**Unclassified**	**Unclassified**	**SAR**

STRUCTURAL/BALLISTIC INSTABILITY AGEOUT MECHANISM IN THE SPARROW MARK 52 SRM

D. I. Thrasher
OL-AC Phillips Laboratory
4 Draco Drive
Edwards Air Force Base, CA 93534

P. R. Empleo
Sparta, Inc.
244 E. Avenue K-4
Lancaster, CA 93535
USA

SUMMARY
A three dimensional finite element analysis and a one dimensional incompressible flow model were used to investigate the interaction between the internal ballistics and the structural grain deformations for the Sparrow Mark 52 rocket motor. The results confirm earlier investigators' conclusions (based on two dimensional structural analysis) that a mechanism exists for pressure spiking driven by choking of the gas flow within the bore cavity due to grain structural deformations. Significant differences were found between the 2D and 3D results, however; the 3D analysis requires a higher propellant modulus to prevent choking under the same analysis conditions.

INTRODUCTION
The Sparrow Mark 52 rocket motor had a history of occasional "pressure spikes" during the ignition transient in test firings at 71 °C. The Mark 52 motor (see Figure 1) was characterized by a 5-lobed star grain configuration and a relatively constrained flow passage.

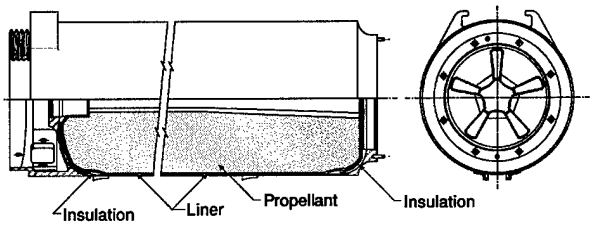

Figure 1. Motor Geometry

Previous analyses of the Sparrow Mark 52 motor had indicated that the anomalies were caused by an interaction between the flow field and the motor structural response, coupled through the pressure/grain deformation relationship. The nonlinear interaction between the two processes can become unstable in these motors if the propellant modulus is low enough, causing the flow to choke near the end of the grain and causing the pressure spike. At the time this analysis was conducted, the frequency of occurrence of pressure spikes in Mark 52 test firings was increasing with motor age, so we were concerned about this phenomenon as a potential ageout mechanism for the motor. Since accelerated aging of the propellant showed a tendency to soften with age, (see Figure 2) it appeared that the tendency for pressure spiking should be age dependent.

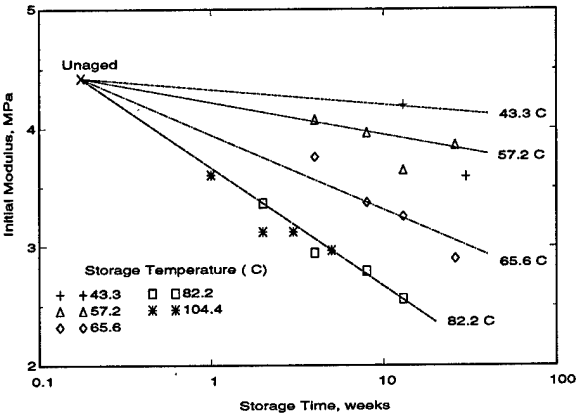

Figure 2. Propellant Accelerated Aging Data

The purpose of the work reported here was to verify previously reported analyses of the problem with an important improvement: while the earlier analyses used axisymmetric ("2D") structural models to represent the propellant grain, we used the TEXGAP-3D program to generate a detailed three-dimensional structural model of the motor.

ANALYSIS PROCEDURE
Figure 3 shows the overall approach that we used to model the structural/ballistic interaction problem. The key parts of the overall model are the geometry model (composed of a burnback model and a structural deformation model) and the flow model. As indicated in Figure 3, the original motor geometry is altered to a burnback configuration by the burnback model. The geometry is further modified by the structural deformation

model to account for the structural deformations (which are defined in terms of a deformation amplitude and the motor head end pressure). The final modified geometry and head end pressure are then fed into the flow model, which computes the pressure distribution. The structural deformation model within the geometry model is a set of empirical relationships based on results from the TEXGAP-3D analysis and other structural analyses.

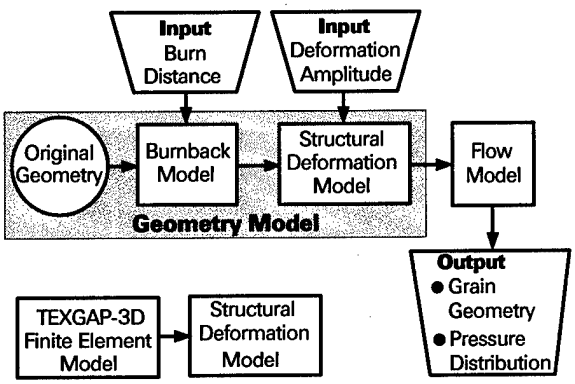

Figure 3. Modeling Approach

Details of the modeling approach are discussed later in this paper.

ASSUMPTIONS

The major assumptions we made are listed separately below for the two main parts of the analysis: the structural analysis and the flow analysis.

Structural Analysis Assumptions

1. All materials in the motor behave either elastically or in a quasi-elastic manner, characterized by effective viscoelastic moduli for the propellant grain, liner, and insulation and by constant values of the bulk modulus of compressibility for these materials.

2. Linear superposition applies for all structural deformations; furthermore the net area change from all contributions (including burning) can be determined by linear superposition of the components of area change.

3. The structural deformations calculated for the original geometry are valid for the burnback geometry.

Flow Analysis Assumptions

1. Friction is negligible.

2. The gas flow is steady and one-dimensional.

3. The gas can be treated as an incompressible fluid.

4. The mass generation rate per unit of undeformed surface area is independent of pressure and location within the propellant grain.

5. Area changes due to structural deformation do not change the mass flow rate per unit of undeformed surface area.

STRUCTURAL ANALYSIS

We used a number of different structural analysis tools in the course of this analysis. The structural models used, and their roles in the overall analysis, are discussed below.

TEXGAP-3D Model

We made a detailed TEXGAP-3D analysis of the motor under the pressure loading shown in Figure 4.

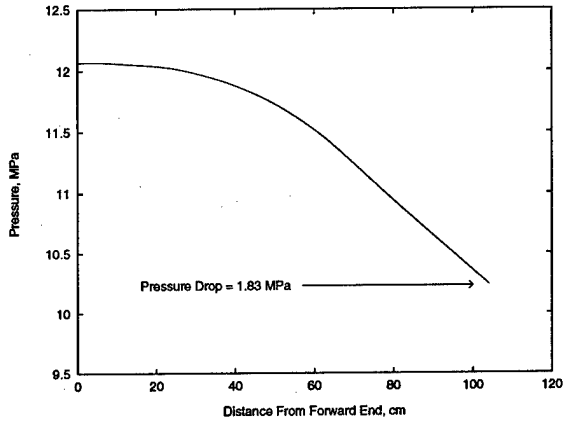

Figure 4. Applied Pressure Load.

The analysis used a total of 492 quadratic-displacement elements to model a basic-symmetry section (a 36-degree wedge) to capture the 5-point slotted geometry of the motor. The elements used to model the insulator, liner, and propellant were the reformulated elements designed for nearly incompressible materials. In addition to the internal pressure load, the boundary conditions included the nozzle ejection load and the igniter ejection load. The deformed geometry of the aft portion (containing 159 elements) of the 3D model is shown in Figure 5.

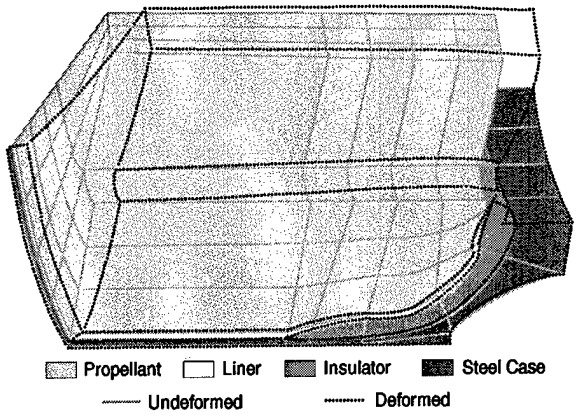

Figure 5. Aft End of TEXGAP-3D Motor Model

Figure 5 shows a primary feature of the grain deflection of the Sparrow Mark 52 motor under the pressure loading of Figure 4; the propellant grain is forced against the aft dome, causing it to bulge inward and constrict the cross sectional area available for gas flow. The constriction of the flow area is evident in Figure 6.

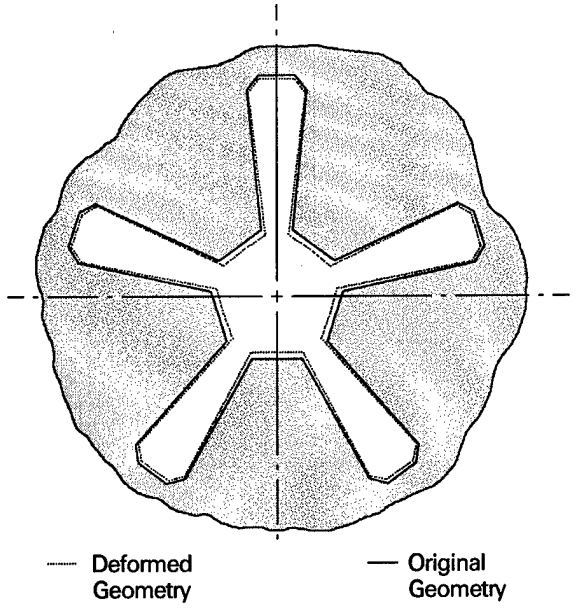

Figure 6. Deformation of Motor Bore

The low modulus of the liner material (white layer in Figure 5), permitting a large shearing deformation of the liner layer, is a key factor in this behavior.

TEXGAP-2D/Approximate-3D Models

We used the TEXGAP-2D/Approximate-3D finite element code to link our analysis to earlier investigations which used two dimensional models. Two geometry models were generated, an axisymmetric equivalent cylinder model (basically the 3D geometry with all material between the slot valleys removed) and an approximate 3D model using slot elements to model the slotted region of the grain. Figure 7 shows the Approximate-3D finite element model.

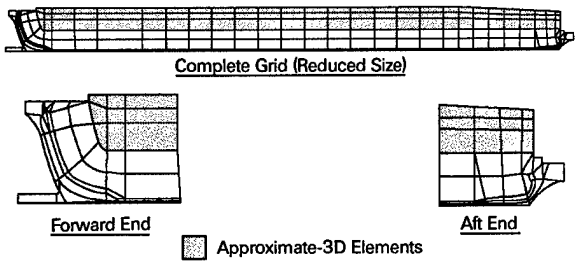

Figure 7. Approximate-3D Finite Element Model

These models used 153 and 237 elements respectively, mostly quadratic-displacement isoparametric elements. Reformulated elements were used for the propellant, insulation, and liner. Both models were subjected to the same boundary conditions as the 3D model.

"QUICK-LOOK" Code Models

The Phillips Laboratory "QUICK-LOOK" code is an upgraded version of a programmable calculator Lamé-cylinder structural analysis program [1] which was ported to the Hewlett-Packard HP-85 microcomputer. The "QUICK-LOOK" code was used to model an equivalent cylinder for the slotted grain as well as the short forward circular port section of the grain which surrounds the igniter. These models were analyzed under generalized plane strain conditions for the thermal and uniform pressure loads.

Material Properties Used

The material properties we used in the various structural analyses are shown in Table 1. The properties used for the nominal analysis (i.e. propellant modulus of 1.55 MPa) are essentially the same as those used by Aerojet in their analysis of the spiking problem. The properties for the propellant, insulation, and liner were considered to represent the lower limits of modulus for these materials. The lower and higher propellant modulus values (0.689 MPa and 3.45 MPa) for pressurization were included to allow scaling of the results for different propellant modulus values. The modulus values used in the "QUICK-LOOK" analyses were based on effective modulus calculations for a specific set of propellant data discussed later in this paper.

Table 1. Mechanical Properties Used in Structural Analyses

	TEXGAP-3D	TEXGAP-2D APPROX-3D	QUICK LOOK
PROPELLANT			
E, MPa	1.55	0.689, 1.55, 3.45	0.35, 1.55*
$\beta^{\dagger}$, MPa	517	517	517
LINER			
E, MPa	0.14	0.14	N/A
$\beta^{\dagger}$, MPa	6894	6894	N/A
INSULATION			
E, MPa	6.895	6.895	N/A
$\beta^{\dagger}$, MPa	10300	10300	N/A
CASE			
E, MPa	200000	200000	200000
ν	0.32	0.32	0.32

* Used for thermal deformation only; used $\alpha = 3.6x10^{-6} cm/cm/^{\circ}C$, $\Delta T = -6.6^{\circ}C$

† Poisson's ratio $(\nu) = 0.5 - E/(6\beta)$ where β is the Bulk Modulus of Compressibility

Application of Structural Analysis Results

The primary result from the 3D model was the radial deflection at the bottom of the slot valley under the pressure load. These results are shown in Figure 8.

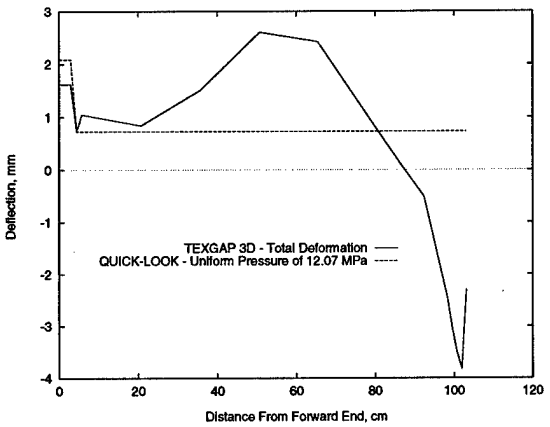

Figure 8. Radial Deflection at Slot Bottom from TEXGAP-3D Analysis

In addition, the deflections at nodal points on the bore surface output by the TEXGAP-3D post processor were analyzed using a specially written microcomputer code to determine the area change under the pressure load.

We used the axisymmetric equivalent cylinder results only for comparison with TEXGAP-3D and the Approximate-3D model. The parameter of interest is the radial deflection, shown in Figure 9.

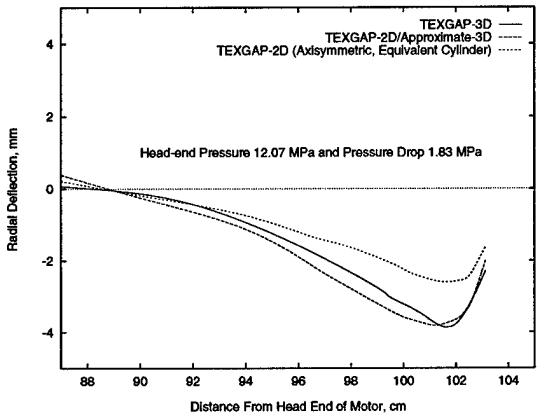

Figure 9. Comparison of 2D and 3D Analysis Results

We used the Approximate-3D model results for comparison with TEXGAP-3D and also (in conjunction with the "QUICK-LOOK" models for uniform pressure) to develop an empirical relationship between the propellant modulus and the radial deflections. As shown in Figure 9, the radial deflection determined by the Approximate-3D model very closely matches the TEXGAP-3D results in the aft end of the motor, while the axisymmetric model's radial deflection is approximately 50% smaller than the 3D model's deflection. These results emphasize the need for a 3D grain analysis.

We used the "QUICK-LOOK" analysis results in two ways: (1) to define the grain response to the thermal load; (2) to provide the uniform pressure component of the radial deflection at the slot bottom so that it could be subtracted from the 3D deformations under the total pressure and thus determine the pressure drop component of the this deflection (see Figure 8). The same procedure was applied to the peak deflection from the Approximate-3D model to determine the relationship between the propellant effective modulus and the pressure drop component of the deflection. The resulting empirical relationship is

$$(\Delta r_{\Delta p})_{max} = [2.1234 + (3.684/E)](\Delta p/1.827) \qquad (1)$$

where $(\Delta r_{\Delta p})_{max}$ is the maximum value of radial deformation, in mm, at the slot bottom with the uniform pressure contribution subtracted out, E is the effective elastic modulus of the propellant in MPa, and Δp is the pressure drop in MPa applied to the grain. This empirical equation fits the Approximate-3D results (and the single 3D result) with a maximum error of 1.2%.

THE GEOMETRY MODEL

The geometry model modifies the motor internal geometry to account for the effects of propellant burning, structural deformation under thermal load, and structural deformation under pressure load. The cross sectional flow area calculated by the geometry model at the nominal analysis conditions (p_0 = 12.07 MPa, Δp = 1.83 MPa, T = 71 °C, and *burn distance* = 0.45 *mm*.) is shown in Figure 10. The relative magnitudes of the various effects are evident in the figure. (The alternative calculations for total deformation–"3D" and "Rigid Fin"–are explained below.

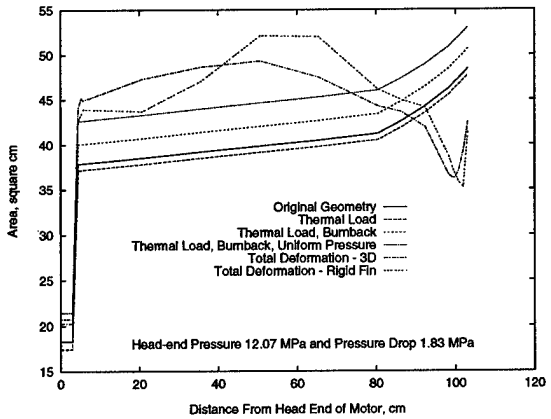

Figure 10. Area Variation Along Motor Length

Overall Geometry Calculations

The geometry model calculates two motor geometry parameters which are needed by the flow model. These parameters are the effective radius of the burning perimeter

at each axial station and the cross-sectional flow area at each axial station.

The burning perimeter, P, is represented in terms of an effective radius, $a(z) = P/(2\pi)$. The effective radius calculation is part of the burnback model. The cross-sectional flow area is:

$$A(z) = A_0(z) + \Delta A_B + \Delta A_{p_o} + \Delta A_{\Delta p} \qquad (2)$$

where $A_0(z)$ is the original flow area, $\Delta A_B(z)$ is the change in flow area due to burnback, and the remaining three terms are the structural deformation components due to thermal load, uniform pressure, and pressure drop, respectively. The detailed models used to generate the individual geometry change components are discussed below.

The Burnback Model

The burnback model consists of the following two equations:

$$a(z) = a_0(z) + x \qquad (3)$$

$$A_B = \pi\left\{\left[a(z)\right]^2 - \left[a_0(z)\right]^2\right\} \qquad (4)$$

where $a_0(z)$ is the original burning perimeter and x is the burn distance, which is specified as an input variable.

The Structural Deformation Model

The structural deformation model computes three structural components of area change: the thermal load component, the uniform pressure component, and the pressure drop component.

Thermal Load Component

The area change due to the thermal load on the motor (temperature soak) is estimated from

$$\Delta A_T = \pi {r_0}^2\left[(1+\epsilon_T)^2 - 1\right] - 2\alpha\Delta T A_0 \qquad (5)$$

where ϵ_T is the hoop strain in an equivalent-cylinder plane strain model of the motor cross section, r_0 is the linear coefficient of thermal expansion of the propellant and ΔT is the difference between the soak temperature and the motor's stress-free temperature. The $\alpha\Delta T$ term arises because the computed strain is the "stress-producing strain," i.e., $\epsilon_T = \Delta r/r_0 - \alpha\Delta T$. The strain level was found to be nearly independent of the modulus over the range considered.

Uniform Pressure Component

The area change due to a uniform pressure equal to the motor head-end pressure is calculated from

$$\Delta A_{p_0} = \pi r_0^2\left[(1+\epsilon_{p_0})^2 - 1\right] \qquad (6)$$

where ϵ_{p_0} is the hoop strain in an equivalent-cylinder plane strain model of the motor cross section and r_0 is defined as in the thermal load case above. Based on our plane strain analysis, the strain level is nearly independent of the modulus over the range considered.

Pressure Drop Component

The area change due the pressure drop through the motor bore is calculated from the TEXGAP-3D analysis results and the uniform pressure plane strain analyses described above. the specific relationship used for this calculation is

$$\Delta A_{\Delta p} = \pi\left[r_0(z) + \Delta r_{\Delta p}(z)\right]^2 - \left\{\pi\left[r_0(z)\right]^2 - a_0)z) + \Delta A_{p_0}\right\}\left[1 + f(z)\Delta r_{\Delta p}(z)\right] \qquad (7)$$

where $\Delta r_{\Delta}p(z)$ is the change in radial displacement at the bottom of the slot valley due to $\Delta p(z)$; $r_0(z)$ and $A_0(z)$ are as previously defined; and ΔA_{p_0} is given by Equation (6). The empirical function f(z) accounts for the effect of grain fin cross-section deformations, and was determined from the deformed and undeformed geometries using the TEXGAP-3D results at each axial station. As used in the structural model, $\Delta r_{\Delta}p(z)$ was calculated from

$$\Delta r_{\Delta p}(z) = \left[\Delta r_0(z)\right]\frac{(\Delta r)}{\left[\Delta r_0(z)\right]_{max}} \qquad (8)$$

where $\Delta r_0(z)$ is the TEXGAP-3D radial deformation with the uniform-pressure component $\Delta r(z)|_{p=p_0}$ subtracted out, and Δr is the input strain amplitude.

Previous analyses of the Sparrow Mark 52 pressure spiking problem were based on axisymmetric ("2D") structural models which were incapable of providing the three-dimensional deformed shape of the propellant grain. As a result the analysts were forced to rely on an assumption termed the "rigid fin" assumption. According to this assumption, the fin cross-section does not deform, but simply translates toward or away from the motor centerline to conform to the radial deflection of the equivalent-cylinder 2D model. We used the rigid fin assumption implicitly in our thermal load and uniform pressure models, where we expected the resulting error to be small due to the essentially plane strain boundary conditions. We considered using the assumption for the pressure-drop component model as well, since it would have simplified the calculations. To determine whether a rigid fin assumption was acceptable, a "rigid fin" model was obtained from our 3D model by setting $f(z) = 0$ in Equation (10). The results (see Figure 10) show that the "rigid fin" assumption does not provide an accurate area determination. We therefore retained the empirical $f(z)$ representation of the ΔA-to-Δr relationship.

THE FLOW MODEL

The theoretical flow model we used was originally derived by Schapery [2] and was applied (in a somewhat simplified version) in earlier analyses of the Sparrow Mark 52 pressure spiking problem.

Based on the assumptions stated earlier along with the conservation of mass and momentum, the pressure drop

equation was found to be

$$\Delta p = p_0 - p = C_2 \left[0.5 \left(\frac{\overline{a}}{A} \right)^2 z^2 + \int_0^z a \frac{\overline{a}}{A^2} z dz \right] \quad (9)$$

where

$$C_2 = C_1 \left[\frac{A_t}{(L\overline{a}_L)} \right]^2 \quad (10)$$

$$C_1 = \frac{1}{\rho} \left(\frac{\dot{m}}{A_t} \right)^2 = p_0 \gamma \left[\frac{2}{(\gamma - 1)} \right]^{\left(\frac{\gamma+1}{\gamma-1} \right)} \quad (11)$$

and

$$\overline{a} = \frac{1}{z} \int_0^z a dz; \quad \overline{a}_L = \frac{1}{L} \int_0^L a dz \quad (12)$$

As before, a is the effective radius of the burning perimeter and p_0 is the motor head end pressure. The other variables are L = *motor length*, A_t = *nozzle throat area*, ρ = *gas density*, $\dot{m}$ = *total mass flow rate*, and γ = *ratio of specific heats for the gas*, the gas being the propellant combustion products. Note that if we assume the variation in the burning perimeter with axial distance to be negligible, we can set $a = \overline{a} = \overline{a}_L$, and Equation (9) simplifies to

$$\Delta p = C_1 \left[0.5 \left(\frac{A_t}{A} \right)^2 \left(\frac{z}{L} \right)^2 + \left(\frac{A_t}{L} \right)^2 \int_0^z \left(\frac{z}{A} \right)^2 z dz \right] \quad (13)$$

Equation (13) is the simplified version used by Schapery and other previous analysts. We compared the results using Equation 13 with those using Equation (9) and found them to be in close agreement except that the simplified model produces an abrupt "dip" in the pressure at the sudden expansion in the forward end of the grain, while the pressure calculated by the more complex model varies smoothly.

We implemented Schapery's model (Equations (9) to (12)) in our flow model by assuming a piecewise-linear variation with z for both a and A. At zero burnback distance, the flow analysis results show a reasonable agreement with the original Aerojet flow analysis results (labeled "Assumed Pressure" in Figure 11).

By repeating the flow analysis with different geometries, we were able to show that the difference between the Aerojet results and our zero-burnback results were caused by Aerojet's approximation of the motor port geometry as a constant-area duct.

Figure 11 shows that the expected burnback of 0.45 mm at a burn time of 0.36 ms produces a significant change in the pressure distribution, indicating that burnback must be included in a realistic analysis of the pressure spiking.

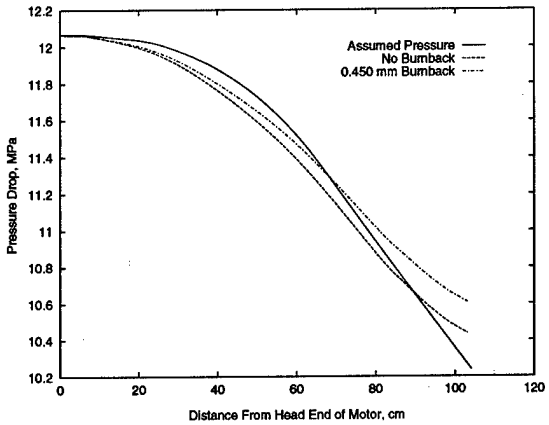

Figure 11. Initial Flow Analysis Results

Figure 12 shows the effects of area changes due to thermal load, uniform pressure, and pressure drop on the calculated pressure distribution for the nominal analysis conditions. From Figure 12, it is evident that the final calculated pressure distribution has a different shape from the assumed distribution, which violates one of our original assumptions. While we did not directly assess the impact of this lack of closure, we think it is minor.

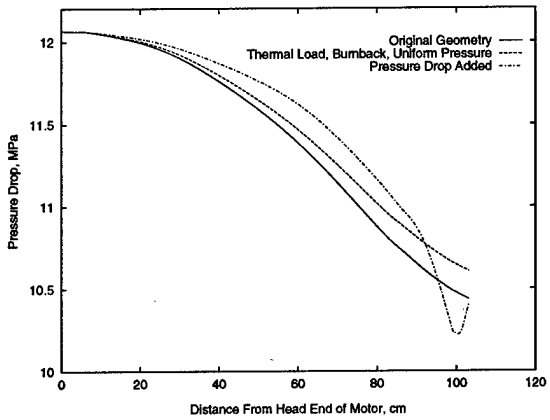

Figure 12. Flow Analysis Results at Nominal Analysis Conditions

RESULTS

Taking the maximum pressure drop from Figure 12 as the relevant parameter to compare to the nominal pressure drop in the original 3D structural model, we were able to attempt a solution of the nonlinear problem that defines the equilibrium pressure drop for the motor. The method used here was based on that used by Glick, Caveny, and Thurman [3] to evaluate the stability of a slotted-tube propellant grain using results from a water-table flow simulation and a propellant grain structural analysis. The method used was to first plot pressure drop as a function of the maximum value of the Δp component of radial displacement, as defined by the flow analysis. We then plotted the maximum Δp component

of radial displacement versus pressure drop, as determined by the structural model (i.e., Equation (1)), and determined where the curves intersect. Failure of the curves to intersect corresponds to an unstable condition that would lead to very large deformations and choked flow at the minimum-area point. This condition would produce a pressure spike.

Incorporation of Actual Mechanical Properties
The process described above is carried out in Figure 13 for a specific set of propellant modulus values based on data from a dissected Mark 52 motor.

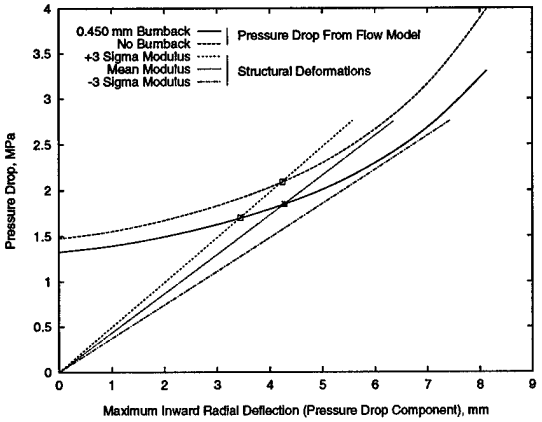

Figure 13. Analysis Results for Ignition at 71 ° C (Head-End Pressure = 12.07 MPa)

The propellant from this dissected motor was very soft. The modulus values were less than half the normally expected values over the entire relaxation spectrum. However, since this propellant (ANB-3109-2) softens with age, the modulus data from this motor (SN 3600646) was selected to obtain a conservative evaluation of the pressure spiking problem. A modified power law relaxation modulus function was determined from the relaxation modulus data using a curve fitting technique. Using this relaxation modulus function, the effective elastic modulus was calculated by carrying out the linear viscoelastic convolution integral for a strain history proportional to the motor pressure during a 71 °C ignition pressurization with a 36-ms duration. The procedure used is described in detail in Reference 4. The resulting modulus values (accounting for the error estimate produced by the curve fit) were

$$+3\ Sigma: \quad E = 2.35 MPa$$

$$Mean: \quad E = 1.76 MPa$$

$$-3\ Sigma: \quad E = 1.32\ MPa$$

Equation (1) is plotted in Figure 13 for the three different modulus values. As shown in Figure 13, the analysis would predict unstable deformations for the mean modulus value if burnback were ignored. However, for the burnback geometry, the analysis predicts only a small chance of instability (i.e., the modulus must be at or near the lower 3-sigma value to cause instability).

CONCLUSIONS

This analysis confirmed the potential for failure of the Sparrow Mark 52 rocket motor through large bore deformations leading to choked flow at the aft end of the propellant grain, supporting the results obtained previously by other investigators. The following specific conclusions are drawn based on our results:

(1) For the motor operating conditions and propellant properties used in this analysis, the structural deformation is marginally stable. Lower propellant modulus or higher burn rate (producing a higher head-end pressure) could trigger unstable deformation. A lower liner modulus would also increase the potential for instability.

(2) Because of the significantly higher deformations, the three-dimensional structural model leads to a substantially lower margin of stability than would be obtained with a two-dimensional structural model.

(3) The TEXGAP-2D/Approximate-3D computer code closely approximated the radial deformations obtained in the aft end of the motor from the TEXGAP-3D code. This result both corroborates the TEXGAP-3D results and shows the usefulness of the Approxi- mate-3D feature of TEXGAP-2D for analyses involving three-dimensional geometry.

REFERENCES

1. Leighton, R., "Quick-Look Structural Analysis Techniques for Solid Rocket Propellant Grains", AFRPL-TR-81-80, Air Force Rocket Propulsion Laboratory, Edwards AFB, CA May 1982.

2. Schapery, R. A., Texas A&M University, Private Communication, September 1983.

3. Glick, R. L., Caveny, L. H., and Thurman, J. L., "Internal Ballistics of Slotted-Tube, Solid-Propellant Rocket Motors," *j. Spacecraft,* Vol. 4, No. 4, April 1967.

4. Thrasher, D. I., and Corbett E., "An Analysis of a Solid Propellant Transient Viscoelastic Response under Motor Ignition Conditions", AFRPL-TR-81-80, Air Force Rocket Propulsion Laboratory, Edwards AFB, CA, January 1982.